Practical Considerations using Weighted-Acceleration Compensation Techniques for Dynamic Force Measurements in Wind Tunnels

Garrett Trowbridge*
The Pennsylvania State University, University Park, Pennsylvania, 16802, United States

Nicholas Vlajic †
The Pennsylvania State University,
Applied Research Laboratory, University Park, Pennsylvania, 16802, United States

Devin Burns ‡
NASA Langley Research Center,
Hampton, Virginia, 23666 , United States

Most wind tunnel force measurement systems are designed and calibrated for high-accuracy static measurements, but may have limited ability to sense dynamic forces and moments. As a means to improve the measurement bandwidth of dynamic forces, researchers have proposed using a weighted-acceleration technique, which uses accelerometer data to compensate and correct for system dynamics. The sum of weighted-accelerations method is attractive as the acceleration data applies a correction to the traditional static measurements. The focus of this paper is on practical aspects of implementing a weighted-acceleration technique in an experimental arrangement. A formulation of the weighted-acceleration methodology is validated on a reduced-order model and demonstrated on a tabletop experiment that serves as a proxy to a wind tunnel force measurement system. As part of this system, a two component normal force and pitching moment balance was designed and fabricated. A static and dynamic calibration of the system was performed, and the weighted-acceleration technique was used to reconstruct impact forces acting on the system. Practical considerations of the experimental design that improve the success of the methodology are discussed.

Nomenclature

a	=	measured acceleration
α	=	rotation of the balance
b_z	=	damping coefficient of balance in translation
b_α	=	damping coefficient of balance in rotation
$\boldsymbol{B}$	=	damping matrix
$\boldsymbol{C}$	=	dynamic calibration matrix
$\boldsymbol{C}_0$	=	static calibration matrix
d	=	distance from the moment center
ϵ	=	strain of balance
$\boldsymbol{\epsilon}$	=	strain of balance time series
F	=	applied force
I_α	=	moment of inertia of test article
k_z	=	stiffness of balance
$\boldsymbol{K}$	=	stiffness matrix
m_z	=	mass of test article

*Undergraduate Student, Department of Aerospace Engineering, and AIAA Student Member.
†Assistant Professor, Applied Research Laboratory.
‡Research Engineer, NASA Langley Research Center.

M = applied moment
$\boldsymbol{M}$ = mass matrix
$\boldsymbol{q}$ = applied force and moment
$\boldsymbol{Q}$ = applied force and moment time series
$\boldsymbol{S}$ = velocity and acceleration time series
v = measured or estimated velocity
$\boldsymbol{x}$ = position of balance
z = translation of the balance

I. Introduction

In wind tunnel testing, measurement of the static forces acting on a test article is traditionally the primary objective of the test. However, dynamic forces are of interest in certain applications wherein the applied forces and moments change with time at rates close to, or faster than the first natural frequency of the system [1]. Applications wherein the forces can vary quickly with time include wind gust measurements, test articles with actuated control surfaces, or unsteady forces such as turbulence [2–4]. Another application where dynamic forces must be accounted for includes short-duration facilities [5–7]. Here, the initial impulse or shock from the tunnel creates vibrations of the measurement system (including the assembly of the test article, force balance, and sting), and these oscillations persist even when the tunnel is operating at steady-state, which can corrupt the static force measurements.

In general, dynamic force reconstruction falls under the classification of inverse problems [4]. For example, the response of the system is well described by a convolution of the applied force and the impulse response of the system. In order to determine the applied force from the measured output, a deconvolution must be performed. Inverse problems are inherently unstable [8, 9] and can lead to unacceptably large errors.

Researchers have proposed a number of methods to correct for these dynamic effects, which can generally be classified into two categories, namely, inverse methods (in both the time and frequency domain) or compensation methods. Note that the compensation methods also require an inversion, but this inversion is typically done in a calibration process, rather than on the data collected for the reconstructed force of interest. Commonly, for both methods, additional instrumentation is required to have a stable inversion. Weighted-acceleration methods are a type of compensation method and, they are an attractive method for a wind tunnel environment, since they serve as corrections to the traditionally collected balance data [10–12].

In this work, we use a weighted acceleration methodology similar to the one initially described in Ref. [13] and a more refined formulation presented in Ref. [7]. Here, we focus on the practicalities of implementing a weighted acceleration approach. Considerations include designing an experiment that satisfies the assumptions of the method, performing scoping measurements in the form of modal analysis of system components, and studying the benefits of additional instrumentation.

II. Experimental Arrangement: Tabletop Test Bed for Evaluating Force Reconstruction Methodologies

A 3D rendering and photograph of the experimental arrangement used to validate the force reconstruction methodologies are shown in Fig. 1. A two-component balance, described in detail in a later section, was designed to measure pitching moment and normal force, and is shown in Fig. 2. The non-metric end of the balance is secured to a stiff right-angle bracket (Thorlabs AP90RL) with four 10-32 socket head cap screws. This support is then mounted to a larger optical breadboard that has isolation mounts to reduce vibrations from the surrounding environment. A modified tombstone block (Thorlabs TS240) is a proxy to a test article that would be used in a wind tunnel and is attached at the metric end of the balance. This block has equally spaced threaded holes so that the locations of the applied forces are known when performing static and dynamic calibrations.

Data are collected from this setup using a NI compact DAQ system, wherein the strain gauges are sampled using a NI-9237 and accelerometers are recorded using a NI-9234. Five accelerometers with nominal sensitivities of 100 mV/g are mounted on top of the test article. Both strain and acceleration data are recorded with time synchronization at 10 kHz for 5 seconds using a custom LabView code. The system presented here will be used to investigate the use of weighted-acceleration compensation techniques for reconstructing dynamic forces.

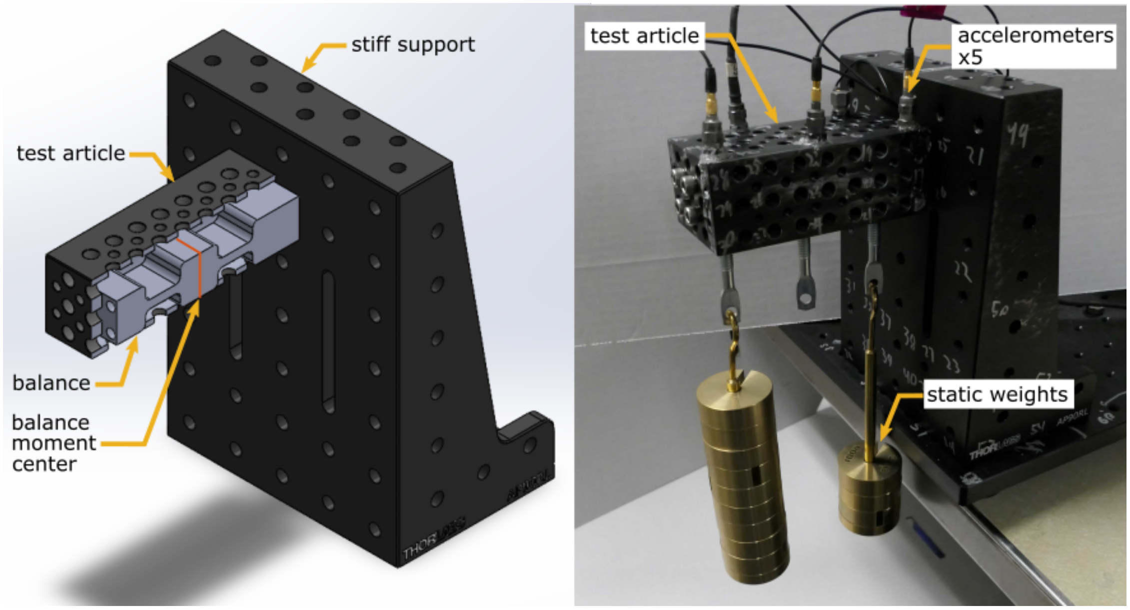

Fig. 1 (left) Rendering of the experimental setup with a cut-away of the test article to show the balance, and (right) experimental arrangement with weights during the static calibration.

III. Force Reconstruction using Weighted-Accelerations

Within this section, we present the generalized weighted-acceleration technique that was described in Refs. [7, 13]. The methodology is presented within the context of a simple two component measuring system consisting of normal force and pitching moment. A simple two degree-of-freedom reduced-order model is used to validate the technique for two different types of inputs, namely, a Gaussian impulse and a step function.

A. Reduced-Order Model: Motivation for a Weighted-Acceleration Approach

A schematic of a simple two degree-of-freedom model with both normal force and pitching moment components that is meant to model the system shown in Fig. 1 is shown in Fig. 3. Assuming the motions between normal force direction (denoted by z) and the pitching moment angle (denoted by α) are uncoupled, the set of differential equations

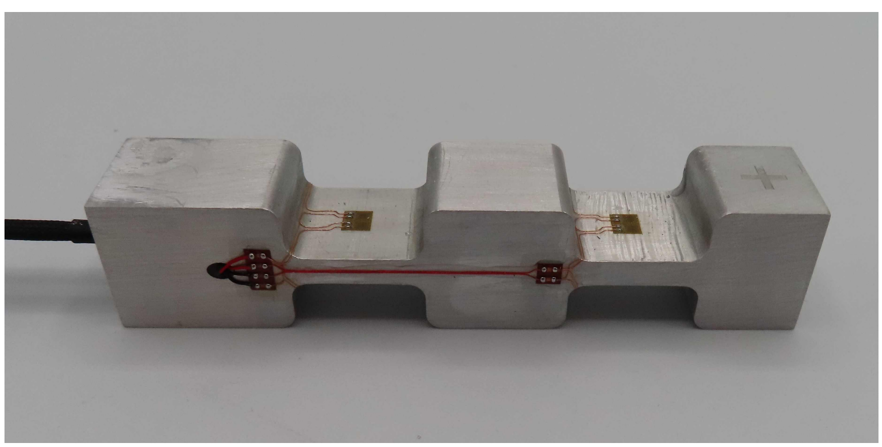

Fig. 2 Photograph of the two component normal force and pitching moment balance. Overall length of the balance is 100 mm.

that model the two degree-of-freedom system are given to be [15]

$$m_z \ddot{z} + b_z \dot{z} + k_z z = F \tag{1}$$

$$I_\alpha \ddot{\alpha} + b_\alpha \dot{\alpha} + k_\alpha \alpha = M \tag{2}$$

The quantity m_z is the effective translational mass in the normal force direction z, while k_z and b_z are the stiffness and damping in the z direction, respectively. Similarly, I_α is the rotational inertia in the α direction, while k_α and b_α are the stiffness and damping in the α direction, respectively. In practice, the two motions are not necessarily independent and coupling exists. For example, as a normal force is applied there may be rotations of the balance. Equations (2) and (1) can then be modified to account for coupling. In matrix notation, these take the form

$$\boldsymbol{M}\ddot{\boldsymbol{x}} + \boldsymbol{B}\dot{\boldsymbol{x}} + \boldsymbol{K}\boldsymbol{x} = \boldsymbol{q}, \tag{3}$$

where the matrices are represented as

$$\boldsymbol{M} = \begin{bmatrix} m_z & 0 \\ 0 & m_\alpha \end{bmatrix}, \quad \boldsymbol{B} = \begin{bmatrix} b_z & b_{z\alpha} \\ b_{\alpha z} & b_\alpha \end{bmatrix}, \quad \boldsymbol{K} = \begin{bmatrix} k_z & k_{z\alpha} \\ k_{\alpha z} & k_\alpha \end{bmatrix}, \quad \boldsymbol{x} = \begin{bmatrix} z \\ \alpha \end{bmatrix}, \quad \text{and} \quad \boldsymbol{q} = \begin{bmatrix} F \\ M \end{bmatrix}. \tag{4}$$

The off diagonal elements of $\boldsymbol{K}$ and $\boldsymbol{B}$ account for coupling between the two directions. The strain $\boldsymbol{\epsilon}$ and output voltage of a balance are proportional to the displacements $\boldsymbol{\epsilon} \propto \boldsymbol{x}$. In a static sense, the time derivatives of Eq. (3) can be dropped and the static equations used for calibration are

$$\boldsymbol{C}_s \boldsymbol{\epsilon} = \boldsymbol{q}, \tag{5}$$

where $\boldsymbol{C}_s$ is a calibration matrix that relates the applied forces and moments to the output strain. Examination of Eqs. (3) and (5) implies that the elements of $\boldsymbol{C}_s$ are proportional to the elements of the stiffness matrix $\boldsymbol{K}$. When using Eq. (5) to make dynamic measurements, the additional mass and velocity effects (captured in Eq. (3) with $\boldsymbol{B}$ and $\boldsymbol{M}$) corrupt the measurement. A further comparison of Eqs. (3) and (5) imply that a correction proportional to an acceleration and velocity can be made to the strain data to correct for these dynamic effects. Methods that attempt to use acceleration data to correct the static measurements are referred to as acceleration compensation techniques.

B. Description of Weighted-Acceleration Technique

The goal of this section is to reconstruct dynamic forces and moments acting on the structure using

$$\boldsymbol{Q} = \boldsymbol{\epsilon}\boldsymbol{C}_0 + \boldsymbol{S}\boldsymbol{C}. \tag{6}$$

Here, $\boldsymbol{Q}$, $\boldsymbol{\epsilon}$, and $\boldsymbol{S}$ are matrices of time series of length n. Note that the calibration matrices are post-multiplied in Eq. (6) rather than pre-multiplied in Eq. (5) for compatibility reasons. For a two-component normal force and pitching moment

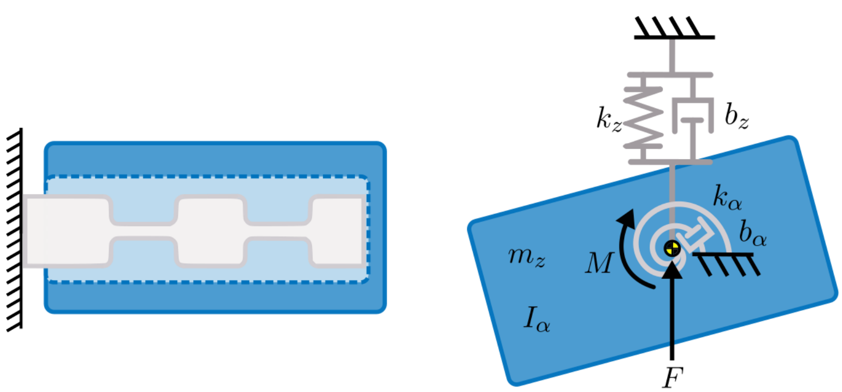

Fig. 3 Representation of the two degree-of-freedom numerical model used to validate the methodology.

measurement system, these matrices take the form

$$\boldsymbol{Q} = \begin{bmatrix} NF_1 & PM_1 \\ \vdots & \vdots \\ NF_n & PM_n \end{bmatrix}, \quad \boldsymbol{\epsilon} = \begin{bmatrix} \epsilon_{1,1} & \epsilon_{1,2} \\ \vdots & \vdots \\ \epsilon_{n,1} & \epsilon_{n,2} \end{bmatrix}, \quad \text{and} \quad \boldsymbol{S} = \begin{bmatrix} v_{1,1} & a_{1,2} & \dots & v_{1,s} & a_{1,s} \\ \vdots & \vdots & \dots & \vdots & \vdots \\ v_{n,1} & a_{n,2} & \dots & v_{n,s} & a_{n,s} \end{bmatrix}. \tag{7}$$

The quantity $\boldsymbol{Q}$ denotes the generalized force and moment vector, which are columns of the normal force (NF) and pitching moment (PM) as a function of time. The matrix $\boldsymbol{\epsilon}$ is a time series of strain measurements that would be sampled from a traditional static balance. The matrix $\boldsymbol{S}$ is a time series of signals from s total sensors that are proportional to both velocity v and acceleration a measurements. In practice, the accelerations are measured from accelerometers and the velocities are integrated from the acceleration data. The matrix $\boldsymbol{C}_0$ is the static calibration matrix of constant coefficients, while the matrix $\boldsymbol{C}$ is a matrix of constant coefficients that is post-multiplied by the velocity and acceleration data $\boldsymbol{S}$ to correct the static measurements. The static matrix $\boldsymbol{C}_0$ is found by applying a series of static forces and moments to the balance, while $\boldsymbol{C}$ is determined in a dynamic calibration by applying known dynamic forces to the test article.

During a static calibration known values of $\boldsymbol{Q}_0$ are applied and the response from strain gauges $\boldsymbol{\epsilon}_0 = \{\epsilon_{0,1}, \epsilon_{0,2}\}$ is measured. Here, the 0 subscript indicates a static measurement, while the second subscript indicates the strain gauge bridge component number (e.g., $\epsilon_{0,1}$ indicates the static response from strain gauge bridge component number 1). The strains within this manuscript are assumed to have the biases while unloaded subtracted out. Typically, a series of static calibration loadings are done to identify the static calibration coefficients. Using superscripts to denote the static calibration loadings, the data can be aggregated into matrices as

$$\begin{bmatrix} \epsilon_{0,1}^1 & \epsilon_{0,2}^1 \\ \vdots & \vdots \\ \epsilon_{0,1}^l & \epsilon_{0,2}^l \end{bmatrix} = \begin{bmatrix} C_{NF,1} & C_{PM,1} \\ C_{NF,2} & C_{PM,2} \end{bmatrix} \begin{bmatrix} NF^1 & PM^1 \\ \vdots & \vdots \\ NF^l & PM^l \end{bmatrix}, \tag{8}$$

or written more concisely as

$$\bar{\boldsymbol{\epsilon}}_0 = \boldsymbol{C}_0 \bar{\boldsymbol{Q}}_0. \tag{9}$$

The over-bar quantities represent collections of a number of measurements. The linear static calibration coefficients contained in $\boldsymbol{C_0}$ are found by least-squares fitting, which is given by the pseudoinverse

$$\boldsymbol{C_0} = (\bar{\boldsymbol{\epsilon}}_0^T \bar{\boldsymbol{\epsilon}}_0)^{-1} \bar{\boldsymbol{\epsilon}}_0^T \bar{\boldsymbol{Q}}_0. \tag{10}$$

Higher order coefficients are typically fit when calibrating balances statically, but these coefficients are typically small compared to the errors induced from system dynamics [14]. Therefore, only a first-order static calibration matrix is generated in this work.

The dynamic calibration matrix is found by rearranging Eqn. (6) and applying the pseudoinverse

$$\boldsymbol{C} = (\bar{\boldsymbol{S}}^T \bar{\boldsymbol{S}})^{-1} \bar{\boldsymbol{S}}^T (\bar{\boldsymbol{Q}} - \bar{\boldsymbol{\epsilon}} \boldsymbol{C}_0). \tag{11}$$

In a similar manner to the static calibration, the over-bars represent a collection of measurements, for example

$$\bar{\boldsymbol{S}} = \begin{bmatrix} \boldsymbol{S}^1 \\ \vdots \\ \boldsymbol{S}^l \end{bmatrix} \quad \text{and} \quad \bar{\boldsymbol{Q}} = \begin{bmatrix} \boldsymbol{Q}^1 \\ \vdots \\ \boldsymbol{Q}^l \end{bmatrix}. \tag{12}$$

In the calibration stage, known dynamic forces are applied and the response of the system is recorded. Here, each $\boldsymbol{S}^i$ represents a time series of the s sensors and each $\boldsymbol{Q}^i$ represent the time series of the applied forces and moments.

A distinction between the work of Refs. [7, 13] and the methodology presented here is the absence of modal filtering in the current work. In the works of Ref. [7, 13], essentially a dynamic calibration matrix is calculated for each mode. For the method presented here, the data are not filtered for each mode to determine a dynamic calibration matrix for each mode; rather, the entire unfiltered time series is used to calculate $\boldsymbol{C}$.

Table 1 Parameter values used in the numerical model.

Parameter	Value	Units
m_z	0.1503	kg
I_α	5.71×10^{-3}	kg m^2
d	0.127	m
k_z	2.29×10^5	N/m
k_α	3.13×10^4	kg m
b_z	0.0226	N/(m/s)
b_α	175	kg m

C. Method Validation using a Reduced-Order Model

The methodology outlined in Section III.B was validated using the two degree-of-freedom model without any simulated measurement noise. System parameters are outlined in Table 1 and are taken from Ref. [15]. Equations (1)-(2) are numerically solved using a fourth order Runge-Kutta method in MATLAB. In the simulation, the stiffness elements k_z and k_α were assumed to be known since in practice, these parameters would be accurately known from a static calibration. Simulations were run using two different applied dynamic forces that represent two different dynamic calibration data sets. The acceleration quantities $\ddot{z}$ and $\ddot{\alpha}$ were used in the analysis as these represent measurements that could be made using accelerometers. The accelerations were integrated to estimate the velocities. Afterward, the methodology presented in Section III.B was used to determine the dynamic calibration matrix $\boldsymbol{C}$.

Two other simulations were run using an applied Gaussian-shaped force and a step force to the model. The $\boldsymbol{C}_0$ and $\boldsymbol{C}$

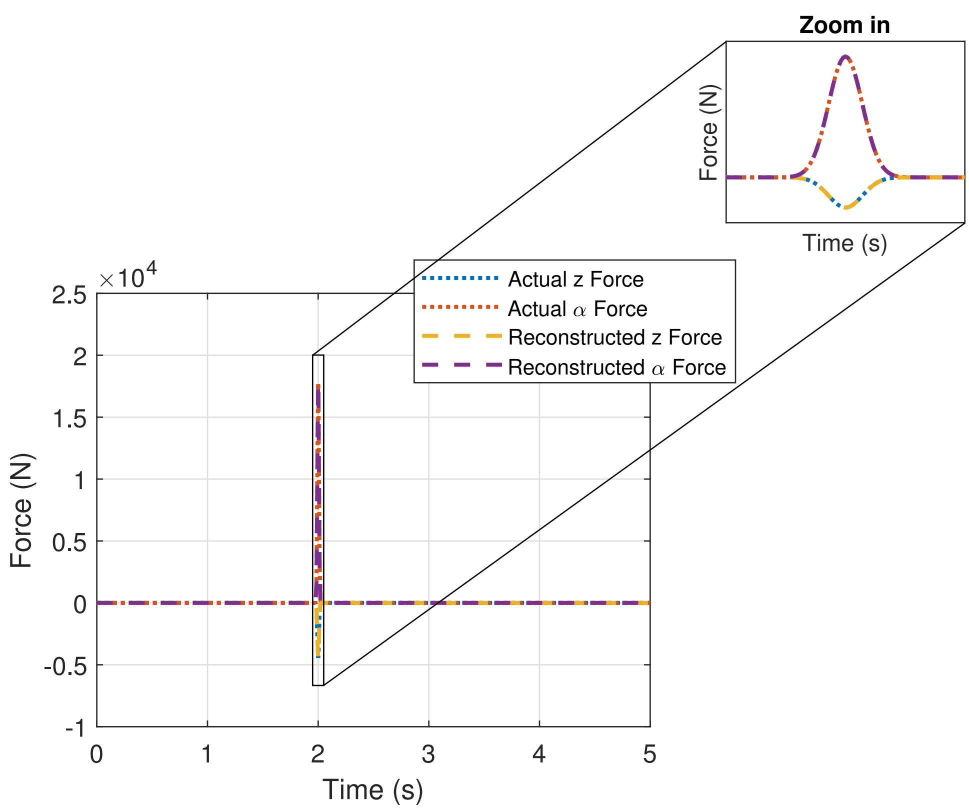

Fig. 4 Simulation results of a reconstructed Gaussian-shape force using the weighted accelerations method.

matrices used in the simulated calibration were then used to reconstruct the force and moments for both cases. Results are shown in Fig. 4 for the Gaussian-shaped force and in Fig. 5 for the step force. In both cases, the reconstructed force and moments compare well with the true values. Although not shown, the percent error is less than 1% over the entire time trace for both cases. These simulations did not include any measurement noise that would be present in practice, nor did they include any additional modes from the test article and supporting structure; however, these results verify that the technique is valid for the given modeling assumptions. Moreover, these results show that accurate results can be achieved without using modal filtering. In the following sections, the methodology is demonstrated on experimental data from the tabletop experiment presented in Section II.

IV. Experimental Methodologies

A. Balance Design Considerations

The balance described in Section II was designed so that it could mount to the stiff support on the fixed end to minimize additional sources of vibration beyond the balance, and the metric end of the balance facilitated the attachment of a proxy test article that also serves as a calibration block. The balance was designed to be longer on the non-metric end so that it would protrude out of the test article.

In order to ensure optimal performance of the transducer, the balance was designed to exhibit specific amounts of strain on the two lands forward and aft of moment center (Fig. 2). Specifically, between 250 and 500 microstrain was desired on both lands when 45 N of normal force is applied and also when 2.8 Nm of pitching moment is applied. The lower limit was established to ensure an acceptable signal to noise ratio, and the upper limit helped ensure the long term performance of the transducer. To meet these requirements, the cross section of the lands ended up being 19.05 mm by 4.45 mm.

The balance was manufactured from a single piece of aluminum 7075-T6 bar stock with nominal modulus of elasticity of 72 GPa and instrumented with N5K-S5054K 5000 ohm transducer class strain gauges. Full wheatstone bridge circuits were installed on both the forward and aft lands.

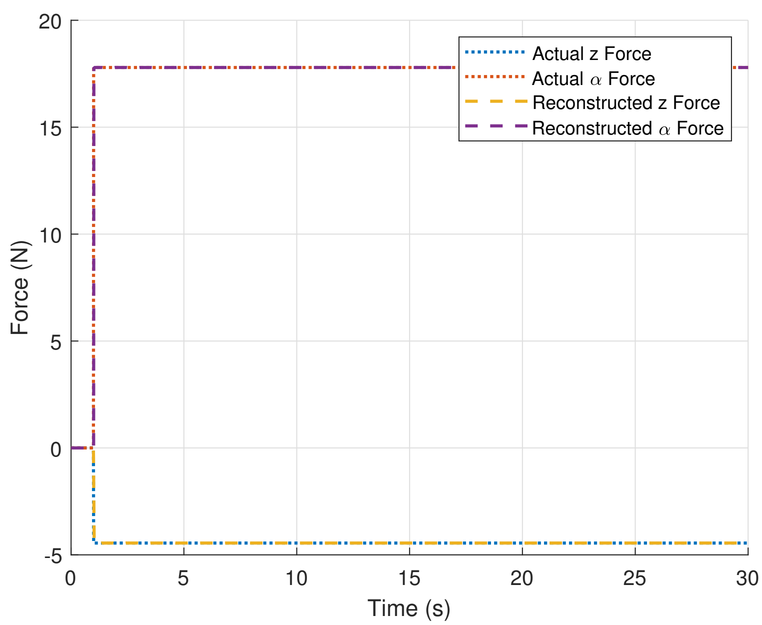

Fig. 5 Simulation results of a reconstructed step force using the weighted accelerations method.

B. Static Calibration

A static calibration was conducted by hanging calibrated weights from various position on the calibration block. Specifically, weights were hung at moment center and 2.54 cm forward and aft of moment center with the balance in both positive and negative normal force orientations. Weights were hung in 1.96 N increments to a maximum normal force application of 19.61 N and a maximum pitching moment of 0.25 Nm. Thus, only 44% of the designed normal force (45 N) and 9% of the designed pitching moment (2.8 Nm) was applied due to experimental limitations. Data was acquired using a NI-9237 bridge card excited at 2.5V. For the static measurements, averaging over 5 seconds was conducted. Figure 6 shows the balance response to normal force and pitching moment. When normal force is applied, the normal force response is pronounced and linear, whereas the pitching moment response is significantly less pronounced. Similarly, when pitching moment is applied the pitching moment response is pronounced and linear, whereas the normal force response is significantly less pronounced.

A total of 110 load applications were part of the static calibration. All data points were used in the construction of a calibration model to obtain $\boldsymbol{C}_0$ per the techniques described in section III.B. The calibration model was then fit to all the calibration data and the residuals between the model fit and calibration data were calculated and are summarized in Fig. 7 for both normal force and pitching moment. Here, the residuals are expressed as a percent of the full scale output for each component. The model fit to normal force results in residuals that do not exceed 0.1% of the full scale applied normal force output. This is noticeably better than the model fit for pitching moment, which has residuals that mainly fall within 0.5% of full scale pitching moment output.

The better performance of the normal force bridge is believed to be primarily attributed to two factors. First, the normal force bridge was loaded to 44% of the design load whereas the pitching moment bridge was only loaded to 9% of the design load. As a result, the normal force bridge exhibited almost twice the output of the pitching moment bridge during the calibration, which helps to improve the normal force residuals as a percent of full scale output. Second, the ability to accurately apply a known pitching moment was likely hindered by the tolerancing of the holes in the calibration block and the limited transfer distances used for the applied moments. For instance, based on the expected tolerances of the calibration block, the 2.54 cm offset distance from moment center (for the pitching moment application) is expected to vary up to 1% (or 0.025 cm), which can result in a measurement uncertainty of the applied pitching moment up to

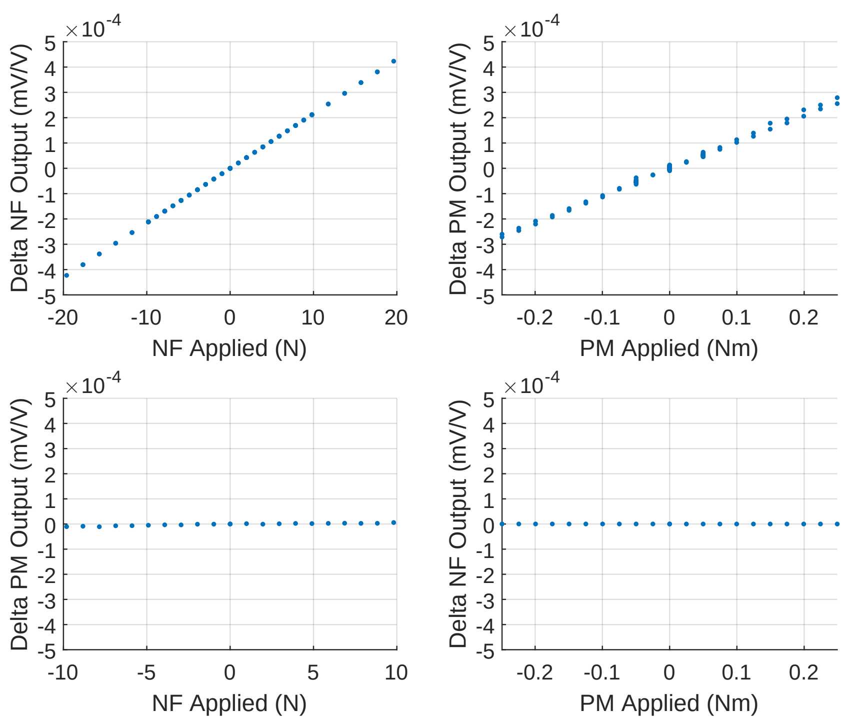

Fig. 6 Quad chart illustrating balance response to normal force and pitching moment.

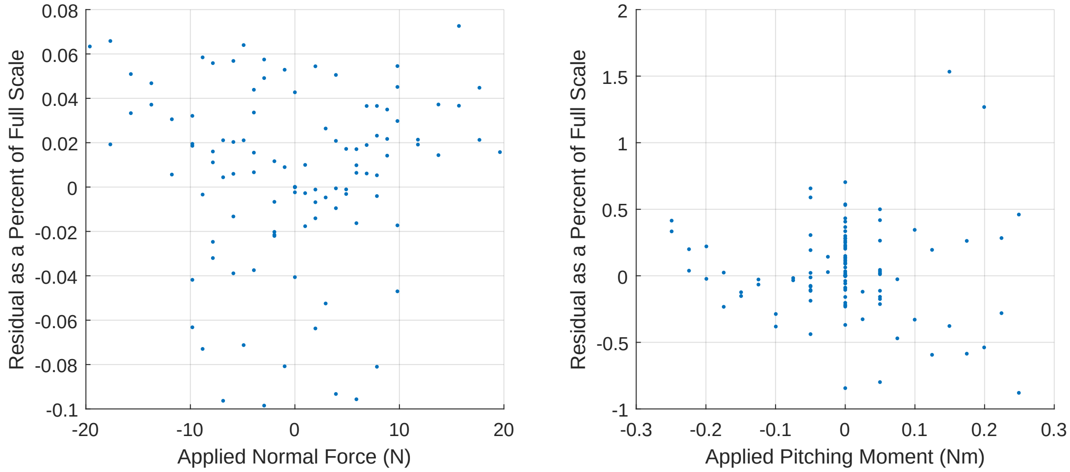

Fig. 7 Residuals for normal force (left) and pitching moment (right) expressed as a percent of full scale.

1%. To improve the pitching moment performance in future work, a larger percentage of the pitching moment design load will be applied, and we will look into applying the load at larger distances from moment center to minimize the relative influence of tolerances.

C. Modal Analysis of System Components

A modal analysis was performed on the experimental arrangement shown in Fig. 1 to identify modes and natural frequencies of the structure. A experimental mesh with 68 hit points is shown in Fig. 8 (right). A roving hammer modal

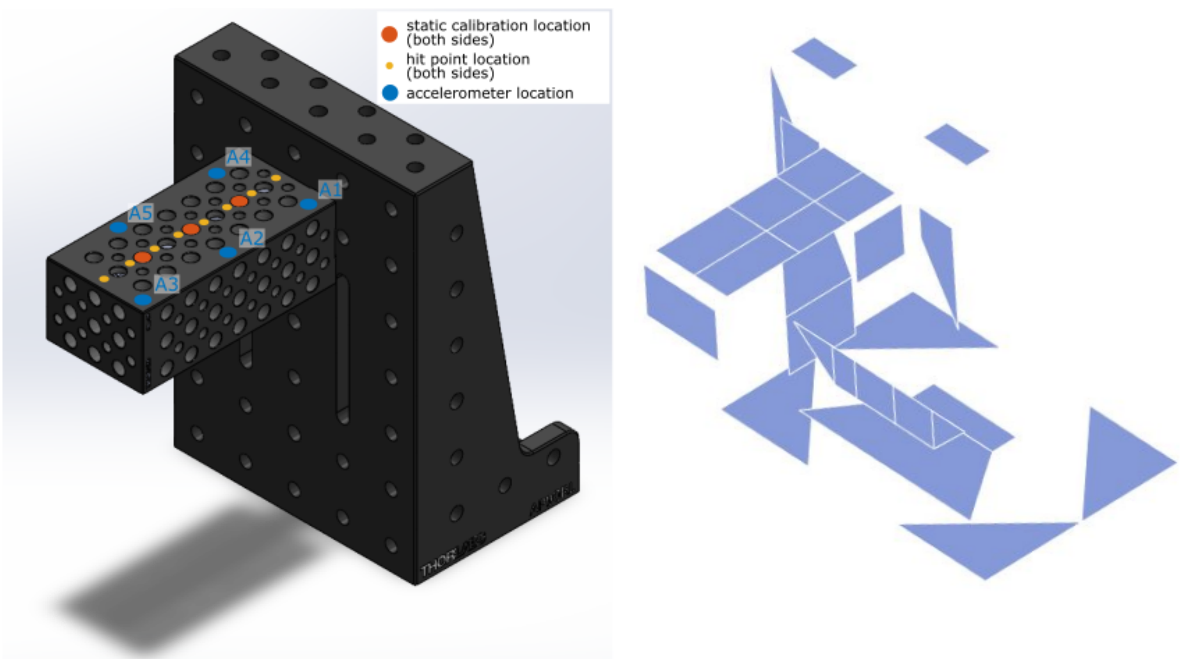

Fig. 8 Geometry of accelerometer, hit point, and static calibration locations (left), and experimental mesh used in the modal analysis (right).

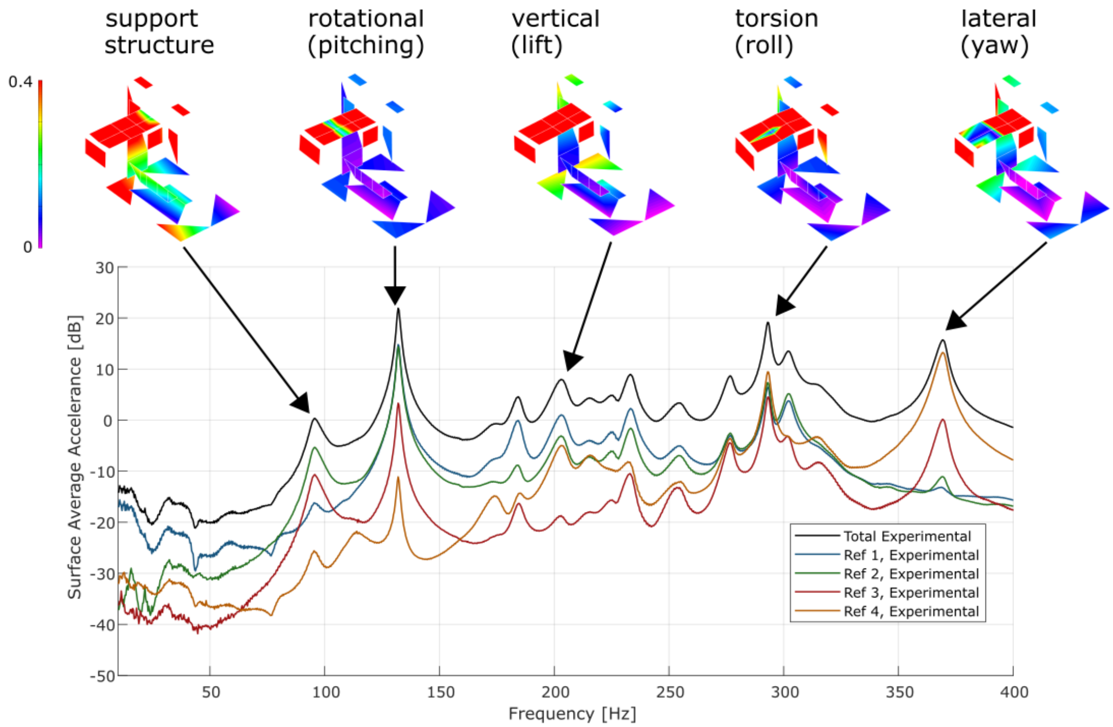

Fig. 9 Surface average acceleration and select mode shapes of the system.

analysis was chosen due to the size of the structure and to reduce the number of sensors. In a roving hammer test, reciprocity is employed so that the accelerometers act as drive points and the hammer hit locations serve as the response points. Note that three accelerometers were used in the modal analysis and were oriented in each of the three Cartesian directions to ensure all three directions were excited. The right-angle stiff support of the balance and the plate that held the stiff support were also struck with the hammer to identify modes of the supporting structure. Modal results that include the surface averaged acceleration and the select mode shapes are shown Fig. 9. The mode at 95 Hz corresponds to motion of the support structure and mounting plate. The most prominent mode with the least amount of damping occurs at 132 Hz and corresponds to pitching motions of the test article. There are roughly five modes between 175 Hz and 240 Hz. The mode at 202 Hz is primarily a normal force motion of the test article. Although the balance was designed for normal force and pitching moment, it still has resonances that correspond to roll and yaw at 293 Hz and 367 Hz, respectively; however, these frequencies are much higher than the pitching moment and normal force directions.

Prior to the modal analysis of the entire assembly, individual components were tested to validate the assumptions in the weighted-acceleration compensation technique. A modal analysis of the test article itself was performed. Here, the test article was suspended by a thin line to attempt to realize freely supported boundary conditions. The first natural frequency of the test article was over 3 kHz, confirming that the block behaves as a rigid body for the frequency range of interest, below 400 Hz.

D. Dynamic Calibration

The experimental arrangement shown in Fig. 1 was dynamically calibrated by applying known dynamic forces at discrete locations indicated in Fig. 8. Forces were applied using an impact hammer [16] with a metal tip, but a cut wire approach also works and in certain applications, may even go to higher bandwidths [17]. Impact hammers typically have different hardness tips to shape the input force profile. The metal tip hammer is the hardest tip and generates forces with the largest bandwidth. Eight points were tapped along the top center line and then again on the bottom center line to have data in both polarities. Applying the forces along the centerline ensures that the pitching moment and normal force directions are the primary directions of excitation with minimal excitation of other modes (torsion, etc.). Each point was hit five times for a total of 80 dynamic calibration points. Data were simultaneously collected from the impact hammer, the two component strain gauge balance, and the five accelerometers.

V. Experimental Results

The weighted acceleration method was validated in Section III.A on a reduced-order model. Within this section, the method is applied to the data collected from the experimental arrangement described in the previous section.

A. Reconstruction of a Pulse-like Force

The impact hammer was used to apply a force by striking the point furthest away from the base on the test article. An estimate of the applied force was then obtained using strain gauge data from the balance, the five accelerometers, and the static and dynamic matrices found in the dynamic calibration. The reconstructed normal force is shown in Fig. 10 (top) while the reconstructed pitching moment is provided in Fig. 10 (middle). The error between the reconstructed force and moment with respect to the true force and moment is expressed as a percentage of the full scale and provided in Fig. 10 (bottom). For comparison purposes, the estimated force when only using a static calibration is shown in Fig. 10 (top and middle). This particular case was chosen because of the atypical applied force and moment shape caused by using a soft hammer tip. The total applied force lasted about 7 ms, but because of the soft hammer tip and the high flexibility of the balance, the strike was not a single impulse and showed a double-hit. In Fig. 10 (bottom), the maximum error is around 3% in normal force and 6% for the pitching moment. When using only the static calibration from the strain gauges, the response contains large errors and oscillations that persist with time.

The Fourier transforms of the time domain data is shown in Fig. 11. The oscillations that were present in the static

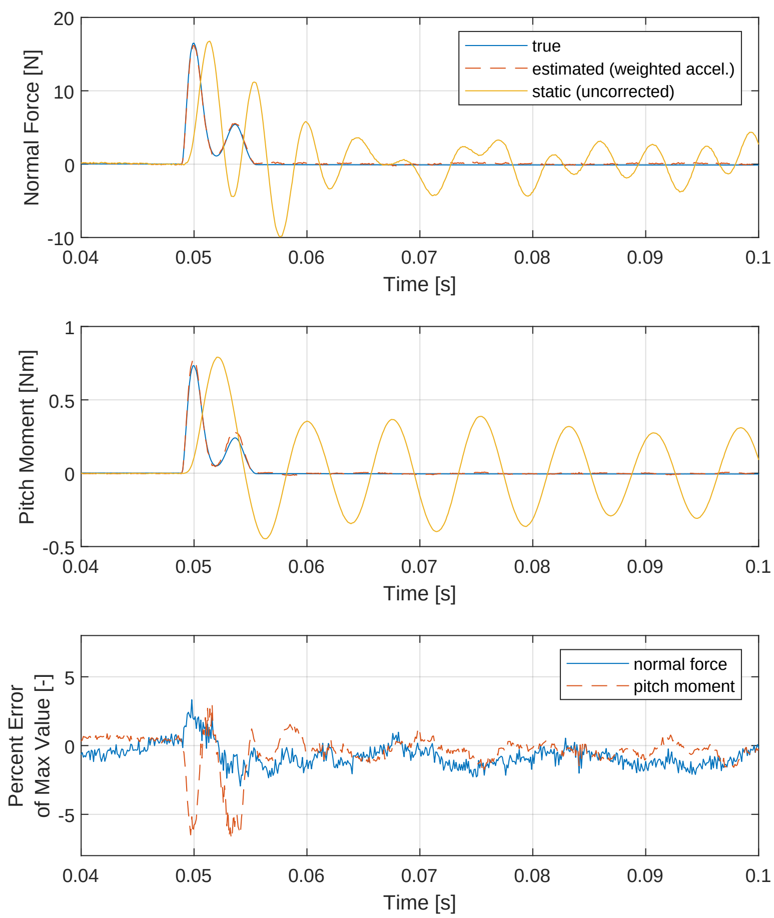

Fig. 10 Reconstructed impulse from an impact hammer in the time domain using five accelerometers.

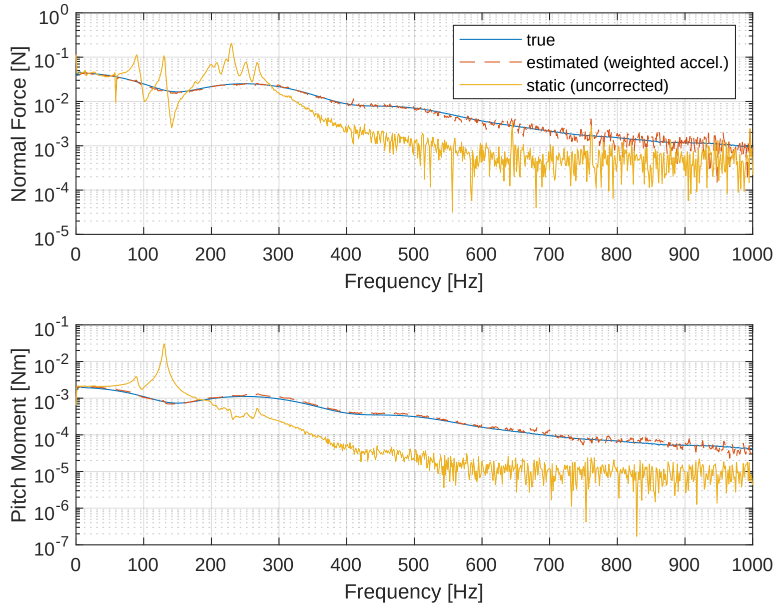

Fig. 11 Reconstructed impulse from an impact hammer in the frequency domain using five accelerometers.

response of Fig. 10 show up as resonances in Fig. 11. The most prominent features show up at approximately 89 Hz, 130 Hz, and 230 Hz. These frequencies correspond to structural resonances that were identified in the modal analysis presented earlier. Here, the reconstructed normal force and pitching moment compare well to the measured applied force. Note that this methodology was able to remove the resonances without doing a mode-by-mode filtering approach.

B. Effects of Additional Instrumentation

The performance of the methodology with subsets of accelerometers is investigated within this section. The force and moment shown in Fig. 10 are reconstructed using accelerometers 1-2, 1-3, 1-4, and 1-5, as shown in Fig. 12. The first 2 accelerometers correspond to A1 and A2 from Fig. 8. Each additional accelerometer adds the sequentially labeled accelerometer from Fig. 8. With respect to the normal force, the two accelerometers are much better than using only the static response (see Fig. 10); however, there are still relatively large errors, approximately 20% of the full scale. The frequency domain results, provided in Fig. 13, show a strong pole-zero near 300 Hz and additional frequency content between 200 and 300 Hz. The 300 Hz mode corresponds to torsion (or a roll mode) of the balance. Adding a third accelerometer does not significantly improve the results. The lack of improvement is attributed to the location of the third accelerometer. Specifically, the location is inline with the first two on the same side of the balance, so that it cannot resolve this torsional mode.

The use of four accelerometers, one of which is not in-line with the others, provided more accurate results. Here, the time domain errors are less than 5% in Fig. 12 and the pole-zero is removed in Fig. 13. Since the fourth accelerometer is on the opposite side of the block as accelerometers 1-3, the configuration is able to remove the torsional (roll) resonant mode. Using five accelerometers does not increase the performance from the four accelerometers by a meaningful amount. For the configuration presented here, the pitching moment is relatively insensitive to the number of accelerometers. Only small improvements to the pitching moment measurement accuracy is observed with additional accelerometers.

While the reconstructed dynamic forces presented here agree reasonably well with the true applied forces, it should be emphasized that the experiment was designed to meet the assumptions of the weighted-acceleration methodology. First, the natural frequency of the test article by itself was much higher than the frequency range of applied forces, so it behaved as a rigid body in the frequency range of interest. Second, the balance was mounted to a stiff support, rather than a less stiff sting as would typically be the case in a wind tunnel measurement facility. Although the supporting

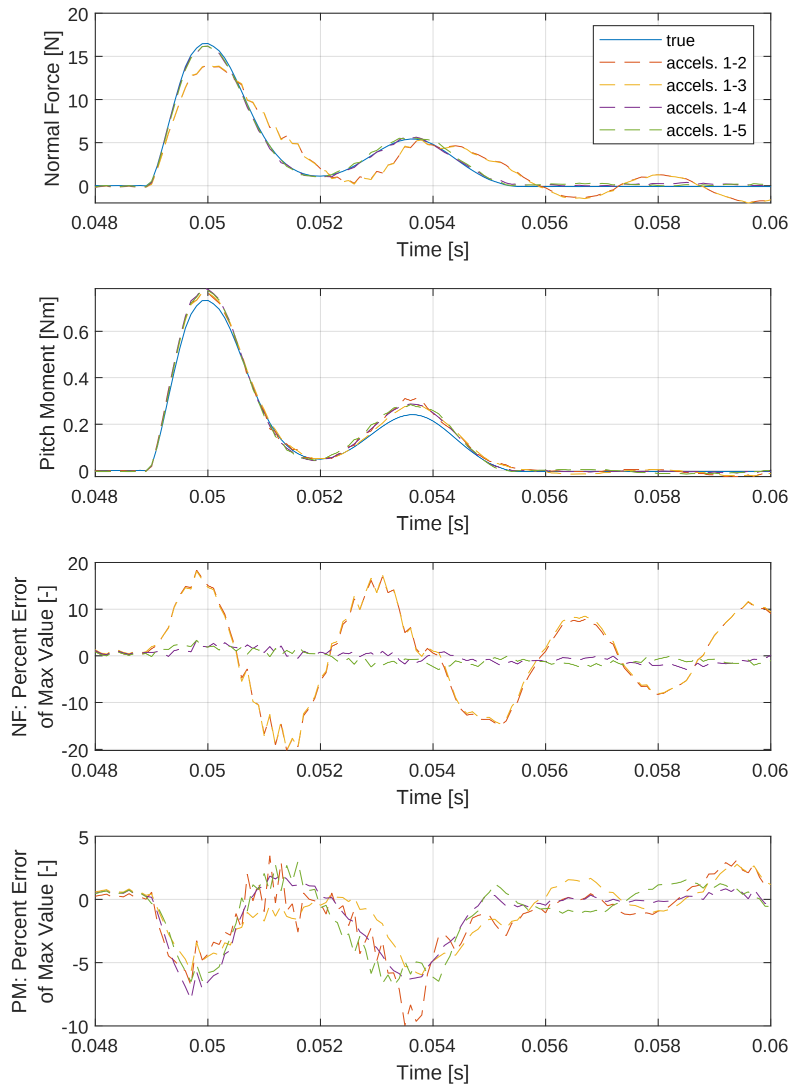

Fig. 12 Reconstructed impulse from an impact hammer in the time domain using five accelerometers.

structure had resonances below the primary normal force and pitching moment natural frequencies, the amplitudes were much lower so that their effects were not pronounced.

It is interesting to point out that even though there were less accelerometers than resonances, the accelerometers were able to remove the modal content shown in the modal response data of Fig. 9 and in the static measurement of Fig. 10. However, the results of this section indicate the the locations of the accelerometers play a role in the quality of the reconstructed force.

VI. Summary and Future Work

Within this manuscript, we summarized and used a weighted-acceleration dynamic force reconstruction technique that was presented in Ref. [7, 13]. The technique was validated on a reduced-order, numerical model for two example

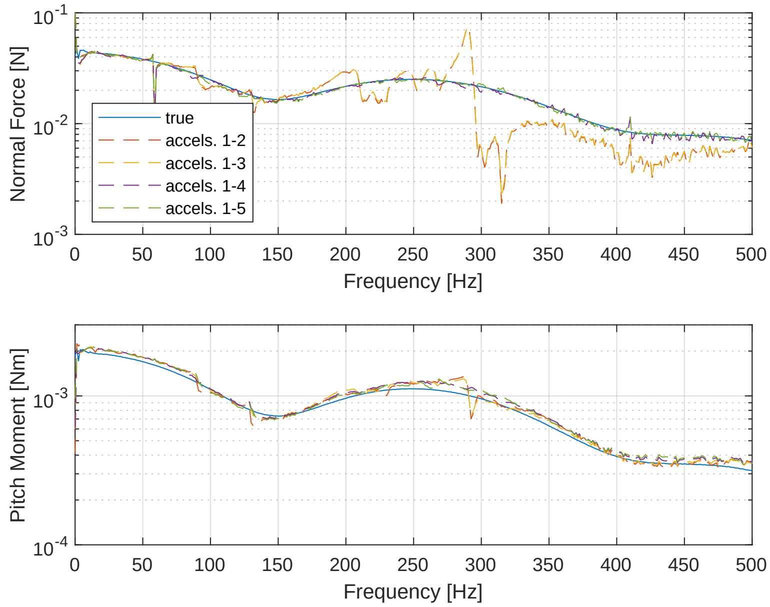

Fig. 13 Reconstructed impulse from an impact hammer in the frequency domain using up to five accelerometers.

cases. The methodology was also applied to a tabletop experimental arrangement that serves as a proxy to a wind tunnel measurement system.

We highlighted a few considerations when implementing the proposed methodology in practice. The technique assumes that the test article is a rigid body and that the balance is rigidly supported, so that the measurement system should be designed to best meet these assumptions. Modal analysis of system components can be done to ensure that the test article behaves as a rigid body in the frequency regime of interest, and to verify that the test article and balance are stiffly supported. The modal results presented here revealed that there were motions of the base, but the amplitude of these motions were small. For the data presented in this paper, a modal filtering approach was not used as was described in Ref. [7, 13]; however, the setup here contained additional accelerometers that were used to reconstruct the force.

The table-top experiment can act as a test bed for scoping out additional methodologies and can be used in future work to challenge some of the assumptions in the weighted-acceleration technique. For example, the methodology assumes that the test article is rigid and that the balance is also rigidly supported. A useful future measurement may evaluate the effects of a flexible sting and test article. These two additional studies may help better quantify the limitations of the weighted-acceleration technique as assumptions about support and test article rigidity break down.

Another aspect of future work may include applying different forces to the structure. Forces with larger bandwidths may be realized using a cut-wire approach [17]. Distributed forces can be applied to the test article using multiple electromagnets as was done to the arrangement in Ref. [20]. In the work of Ref. [20], the distributed forces were applied using a series of electromagnets that excited permanent magnets that were attached to the structure. The test article was calibrated using an impact hammer, which applies forces at a single point; however, in a wind tunnel measurement system, distributed forces would be acting on the body.

Acknowledgments

The authors would like to thank Mr. Keith Rice (Penn State Applied Research Lab) for developing the software used to collect data from the system described within this manuscript. The NASA intern program facilitated Garrett Trowbridge's support and the NASA Hypersonic Technology Project provided Devin Burns's support.

References

[1] Vlajic., N., and Chijioke, A., *An Introduction to Dynamic Force Metrology*, NCSLI, 2018. https://doi.org/16879851, URL https://ncsli.org/store/viewproduct.aspx?id=16879851.

[2] Gorbushin., A., Kozik., A., and Anokhina., E., *Non-stationary load measurement using six-component strain-gauge balances*, ScienceDirect, 2023. https://doi.org/10.2514, URL https://arc.aiaa.org/doi/abs/10.2514/6.2023-2700.

[3] Jones, Z., and Vlajic, N., "Reconstruction of Unsteady Lift Force Measurements Using Non-Dimensional Scaling Optimization," *Experimental Techniques*, 2024, pp. 1–14.

[4] Burns., D. E., Vlajic., N., Chijioke., A., and Parker, P. A., *Aerodynamic Metrologists Guide to Dynamic Force Measurement*, ARC, 2022. https://doi.org/C036676, URL https://arc.aiaa.org/doi/10.2514/1.C036676.

[5] Simmons, D., Gothard, W. D., Molinaro, N. J., and Meritt, R. J., "Wind Tunnel Balance Development for Ludwieg Tube Facilities," *AIAA AVIATION FORUM AND ASCEND 2024*, 2024, p. 4285.

[6] Mee, D. J., "Boundary-layer transition measurements in hypervelocity flows in a shock tunnel," *AIAA journal*, Vol. 40, No. 8, 2002, pp. 1542–1548.

[7] Draper III, J., *Dynamic Force Measurement in Hypersonic Wind Tunnels*, University of Maryland, 2019. https://doi.org/https://doi.org/10.13016/aue2-8a7k, URL https://drum.lib.umd.edu/items/37bcfdb2-e345-4010-8454-4876b97c8ab5.

[8] Hansen, P. C., *Discrete inverse problems: insight and algorithms*, SIAM, 2010.

[9] Vogel, C. R., *Computational methods for inverse problems*, SIAM, 2002.

[10] Gregory, D. L., Priddy, T. G., and Smallwood, D. O., "Experimental determination of the dynamic forces acting on non-rigid bodies," *SAE Transactions*, 1986, pp. 1226–1236.

[11] Carne, T. G., Mayes, R. L., and Bateman, V. I., *FORCE RECONSTRUCTION USING THE SUM OF WEIGHTED ACCELERATION TECHNIQUE MAX-FLAT PROCEDURE*, OSTI, 1994. https://doi.org/10115211, URL https://www.osti.gov/servlets/purl/10115211.

[12] Carne, T. G., Bateman, V. I., and Dohrmann, C. R., "Force reconstruction using the inverse of the mode-shape matrix," *International Design Engineering Technical Conferences and Computers and Information in Engineering Conference*, Vol. 6296, American Society of Mechanical Engineers, 1991, pp. 9–16.

[13] Draper III., J., Lee., S., and Marineau, E. C., *Development and Implementation of a Hybrid Dynamic Force Measurement System at AEDC Tunnel 9*, AIAA, 2017. https://doi.org/10.2514, URL https://arc.aiaa.org/doi/10.2514/6.2017-1593.

[14] Rhew, R. D., and Parker, P. A., "Wind Tunnel Balance Calibration: Are 1,000,000 Data Points Enough?" *International Symposium on Strain-Gage Balances*, 2016.

[15] Buehrle, R., *SYSTEM DYNAMIC ANALYSIS OF A WIND TUNNEL MODEL WITH APPLICATIONS TO IMPROVE AERODYNAMIC DATA QUALITY*, NASA, 2012. https://doi.org/19970015640, URL https://ntrs.nasa.gov/citations/19970015640.

[16] Vlajic, N., and Chijioke, A., "Traceable calibration and demonstration of a portable dynamic force transfer standard," *Metrologia*, Vol. 54, No. 4, 2017, p. S83.

[17] Mee, D. J., "Dynamic calibration of force balances for impulse hypersonic facilities," *Shock Waves*, Vol. 12, 2003, pp. 443–455.

[18] Vlajic, N., and Chijioke, A., "Impact mechanics parametric studies with applications to dynamic force calibration," *International Design Engineering Technical Conferences and Computers and Information in Engineering Conference*, Vol. 58202, American Society of Mechanical Engineers, 2017, p. V006T10A006.

[19] Bruns, T., Kumme, R., Kobusch, M., and Peters, M., "From oscillation to impact: the design of a new force calibration device at PTB," *Measurement*, Vol. 32, No. 1, 2002, pp. 85–92.

[20] Jones, Z., and Vlajic, N., "An experiment for the validation of force reconstruction techniques on flexible structures," *Experimental Techniques*, 2024, pp. 1–18.